RSC Advances

PAPER

View Article Online
View Journal | View Issue



Cite this: *RSC Adv.*, 2017, **7**, 15553

# Bio-inspired hierarchically structured polymer fibers for anisotropic non-wetting surfaces†

M. Yunusa,[ab] F. E. Ozturk,[ab] A. Yildirim,[ab] U. Tuvshindorj,[ab] M. Kanik[ab] and M. Bayindir*[abc]

Received 12th December 2016
Accepted 2nd March 2017

DOI: 10.1039/c6ra28111g

rsc.li/rsc-advances

We demonstrate a rice leaf-like hierarchically textured polymer fiber array for anisotropic non-wetting surfaces. To provide superhydrophobicity in addition to the anisotropic behavior, fiber surfaces are spray coated with organically modified silica nanoparticles. The resulting micro/nano hierarchically structured fiber surfaces demonstrate anisotropic non-wetting properties. We designed various fiber architectures for droplet transportation, mixing, and guiding exploiting the scalability of the fiber texture during thermal drawing; optional nanoparticle surface modification; and inherent flexibility of the fibers.



Anisotropic non-wetting is the tendency of drops to move along a single preferred direction on a surface without wetting it.[1–6] This unidirectional droplet repellency occurs on many natural surfaces for various purposes; for instance, autonomous self-cleaning of lotus leaves, radially outward propulsion of droplets on butterfly wings, hydrodynamic locomotion of water-strider legs, and efficient rain water collection on rice and bamboo leaves.[7–12] The remarkable display of droplets mobility and guidance on biological surfaces is achieved particularly by the use of advanced surface features including ordered micro/nano-scale morphology, and a hydrophobic surface chemistry.[13–15] The realization of artificial surfaces with special anisotropic non-wetting capability is inspiring for the development of self-cleaning surfaces, droplet microfluidics, droplet micro-reactors for precise chemical and/or nanomaterial synthesis, and droplet transport at precise volumes.[16–19] Several methods have been developed to fabricate functional anisotropic surfaces. For example, photolithography is utilized to pattern re-entrant structures such as microgrooves and pillars on various materials (*e.g.*, silicon and polymer),[1,20] and UV treatment on stretched polydimethylsiloxane (PDMS) surfaces which upon releasing forms microscale ripple (wrinkle) pattern.[21–24] Other techniques of interest are polymer imprinting,[25] plasma etching,[26] electrospinning,[27] and femtosecond laser micromachining.[28,29] In addition, fibers are interesting alternative materials for harnessing liquid–solid interactions. Tubular or ribbon shaped micro-fibers were fabricated for microfluidic applications using thiol click chemistry, followed by surface modification with reactive groups.[30,31] However, there are some limitations posed to the global utilization of these methods such as cost-effectiveness, feasibility in large scale production, flexibility of the product, and applicability to large area. Thus, demand for facile and robust fabrication techniques to address these limitations has increased in recent years.

In this work, we reported production of surface textured polymer micro-fibers in kilometers length scale that have perfectly aligned micro-structures on their surfaces using a well-established thermal drawing method.[32] With this new technique, we are not restricted to material choice, and therefore several engineering polymer fibers can be produced. In addition, we demonstrated the preparation of large-area anisotropic non-wetting polymer surfaces analogous to the rice leaf surfaces using both the polyetherimide (PEI) and biocompatible polycarbonate (PC) fibers (Fig. 1). Tens of meters long fibers with perfectly aligned micro-scale features were drawn from a pre-textured polymer rod. The fibers have diameters in the range of 200 μm to 500 μm and parallel micro-grooves of a few dozen micrometers along their whole length. Hydrophobic nanometer scale roughness was introduced over the ordered micro-scale

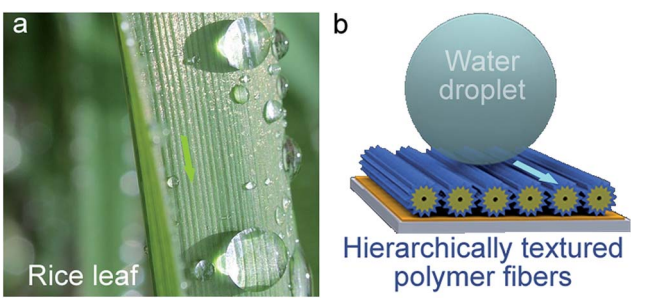


Fig. 1 Directional water transport on hierarchically textured superhydrophobic (a) rice leaf and (b) polymer fiber array.

[a]*UNAM – National Nanotechnology Research Center, Turkey*
[b]*Institute of Materials Science and Nanotechnology, Turkey*
[c]*Department of Physics, Bilkent University, 06800 Ankara, Turkey. E-mail: mb@4unano.com*

† Electronic supplementary information (ESI) available. See DOI: 10.1039/c6ra28111g

grooves on the fibers by coating with organically modified silica (ORMOSIL) nanoparticles.[33,34] Functional anisotropic surfaces of different architectures were constructed by fixing the fibers on paperboard, polymer, and glass substrates using double sided adhesive tape.

The scalability of the fibers and optional nanoparticle surface modification enable construction of variety of fiber surfaces with different wetting characteristics. Mobility of water droplets on the rough fiber surfaces is highly dependent on the wetting regime on the surfaces. We have demonstrated Wenzel and Cassie models on the fiber surfaces. By definition, Wenzel model[35] is regarded as homogeneous wetting regime on rough surface when liquid is in intimate contact with a solid surface. Also, Wenzel droplets are found to be highly pinned to the interacting surface. According to Cassie model,[36] air can remain trapped beneath the droplet, which results in superhydrophobic behavior. This model is considered to be heterogeneous wetting due to the composite formation of solid/air composite on the rough or microstructured solid surface. Roughness increases the surface area of a solid which enhances hydrophobicity. Even though surface chemistry plays a crucial role in wetting, it cannot generate contact angle (CA) as high as 160° without the existence of surface roughness. We demonstrated droplet transport as a proof of concept using sticky hydrophobic and roll-off superhydrophobic surfaces, droplet guiding on fiber track, and a simple protein assay with colliding droplets as examples of droplet manipulation with alternative surface designs for microfluidics application.

## Experimental

### Preform preparation

Initially cleaned and kept in vacuum at 120 °C for a day, PEI film (AJEDIUM; 100 μm thickness and 35 cm width, RESIN – ULTEM 1000-1000) was tightly rolled around a Teflon rod under a clean pressure flow hood, attaining a cylindrical PEI rod of 3 cm in diameter and 20 cm in length. The rolled PEI film and the Teflon rod were introduced into a consolidator (furnace) to fuse the PEI film thermally above its glass transition temperature, $T_g$ (216 °C) under vacuum at $8 \times 10^{-3}$ torr. Two heating regimes were applied to obtain a hollow core solid PEI preform. In the first regime, the rolled PEI film and the Teflon were heated to 180 °C at a rate of 15 °C $min^{-1}$ and kept at this temperature for 4 h. In the second regime, the temperature was increased to 257 °C at a rate of 2 °C $min^{-1}$ and kept in this temperature for 45 minutes to achieve consolidation. Finally, the inner Teflon rod was removed and we obtained a hollow core PEI preform. In order to introduce the groove structure, the hollow core preform was mechanically structured on a lathe by rotating the preform at some angle and knurling its surface. At the end of this operation, 20 evenly distributed v-grooves where patterned on the surface of the preform. The same operation was applied during preparation of PC preform which is identical to the PEI preform. However, consolidation parameters varied for PC preform which has $T_g$ of 147 °C, and therefore different temperature regime was applied. During the first heating regime, rolled PC film and the Teflon rod were heated to 140 °C at a rate of 15 °C $min^{-1}$ and kept at this temperature for 4 h. In the second regime, the temperature was increased to 186 °C at a rate of 2 °C $min^{-1}$ and kept in this temperature for 30 minutes.

### Thermal fiber drawing

Macroscopic v-grooved polymer preform (star-shaped preform) was drawn thermally in a fiber tower. The preform was fed into a furnace vertically with a constant speed of 8 mm $min^{-1}$. The furnace was at a high temperature (approximately 305 °C for PEI and/or 230 °C for PC preform) whereby the preforms soften. Then, mechanical stress was applied to the preforms with a constant speed motor and stretched to a length of tens of meters with varying diameters down to microscale. Precise tuning of the mechanical stress enabled the control of the fiber size.

### ORMOSIL nanoparticle preparation

Methyltrimethoxysilane (MTMS), oxalic acid and ammonium hydroxide (25%) were purchased from Merck (Germany), dimethyl sulfoxide (DMSO) and methanol were purchased from Carlo-Erba (Italy). All chemicals were used as received. ORMOSIL colloidal nanoparticles were prepared according to our previous study.[33,34] Initially, 1 mL MTMS was dissolved in 2 mL DMSO, and then 0.5 mL of oxalic acid solution (10 mM) was slowly added to the mixture and stirred for 30 min. Then 0.42 mL of ammonia solution (25%) and 0.19 mL of water in 5 mL of DMSO were added, and the solution was stirred for 15 min again. In the end, the solution was left for gelation at 25 °C. The gel is typically formed in about one hour. Approximately 20 mL of methanol was added onto the prepared gel and incubated for at least 6 hours at 25 °C to remove the DMSO and unreacted chemicals. This procedure was repeated 4 times to ensure complete removal of DMSO and chemical residues. Methanol (12 mL) was added onto the gel and sonicated using an ultrasonic homogenizer for 45 s at 20 W power to obtain ORMOSIL colloidal suspension which is suitable for nanoporous thin film deposition.

### ORMOSIL nanoparticle coating

Fibers were spray coated by using spray gun Lotus BD-132A; nozzle diameter 0.3 mm, and fluid cup capacity 7cc filled with ORMOSIL nanoparticle solution. Coating time was 2–3 s with pressurized nitrogen gas passing through the gun at 2 bar. After coating the fibers, they were left to dry at room temperature.

### Characterization

A contact angle meter (OCA 30, Dataphysics) was used for the measurement of static contact angle. Laplace–Young fitting was applied to the contact angle measurements. Videos from fiber track, droplet collision and coalescence were recorded using a Sony HDR-CX305E digital camera at 200 fps. Topography of the fibers were investigated with scanning electron microscopy (E-SEM; Quanta 200F, FEI). Atomic force microscopy (AFM; XE-100E, PSIA) was used in noncontact mode to characterize the surface morphology and roughness of the nanoparticle coated

 

fibers. Surface roughness (rms) values were calculated from three separate AFM images. ORMOSIL nanoparticles were investigated with Transmission Electron Microscope (TEM) (Tecnai G2-F30, FEI) operated at 200 kV. TEM samples were prepared by diluting ORMOSIL suspension in methanol. And then, a drop of the solution was placed on a holey carbon-coated copper grit.

## Results and discussion

### Fabrication of surface textured polymer fibers with micro-scale parallel grooves

Polymer fibers are thermally drawn at elevated temperature – higher than their glass transition ($T_g$).[32] Star-shaped fibers were produced from v-grooved preform (Fig. S1†) by thermal drawing under appropriate mechanical stress and temperature profiles. *In situ* diameter control of fiber is achieved by precisely tuning mechanical stress (*i.e.*, increasing or decreasing the motor speed). PEI or PC fibers of several meters length which preserved the star-shaped grooves at varying diameters (ranging from 200 μm to 500 μm) were produced (Fig. 2a). SEM images of the PEI fibers show the star-shaped cross sections and parallel grooves of PEI fibers with 200 μm and 500 μm diameters in Fig. 2b-i and ii. Even the smallest fiber of 200 μm size preserved the v-grooves at the micro-scale; the groove widths and heights are about 30 and 20 microns, respectively, at a 150-fold size reduction of the preform. A bundle of several meters long grooved PEI fiber is shown in Fig. 2a-inset demonstrating their flexibility and high yield of this method. PEI fibers with smooth surfaces were fabricated to compare the groove effect on wettability of the fibers (Fig. S2a and b†). The fiber drawing method is facile and applicable to many engineering polymers. Fig. S2c† shows SEM image of star-shaped PC fibers with microgrooves similar to PEI fibers.

### Introduction of nano-scale roughness on the fiber surfaces

Hydrophobic ORMOSIL nanoparticles[33] were spray-coated on the fiber surfaces to introduce an additional nano-scale roughness (Fig. S3†). The ORMOSIL nanoparticles were homogeneously distributed, forming a continuous porous layer within the asperities as seen in the SEM micrographs (Fig. 2c). Transmission electron microscope (TEM) imaging shows that

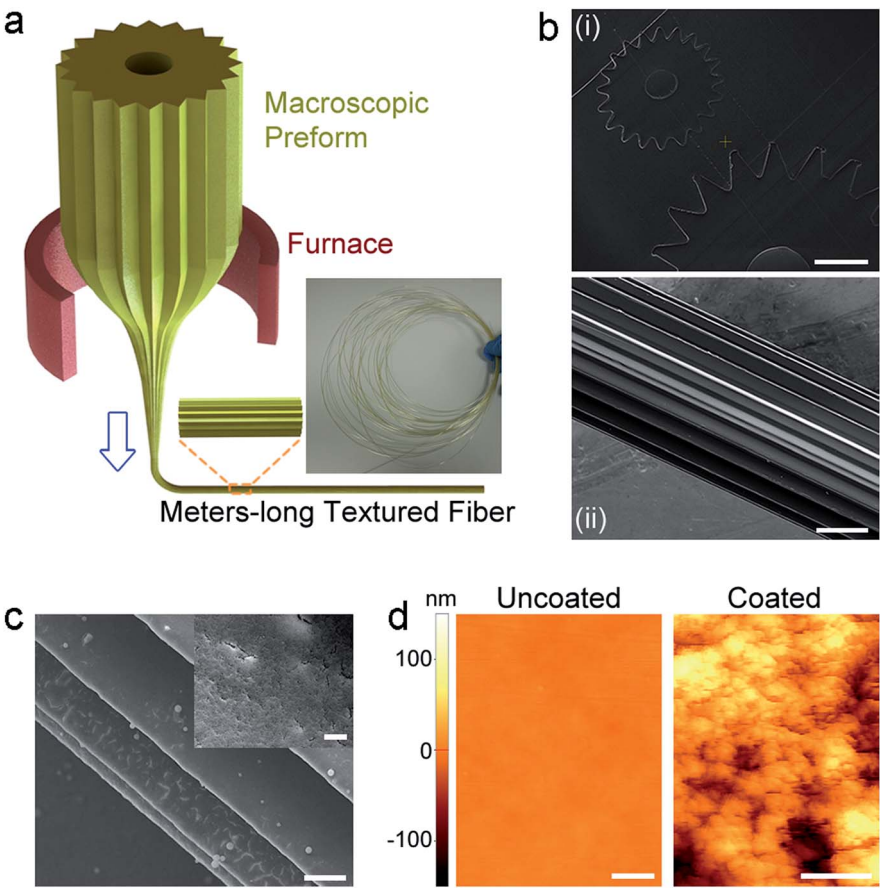


Fig. 2 Fabrication scheme of grooved microfibers and surface modification with nanoparticle coating. (a) Thermal drawing of grooved microfibers from the macroscale star-shaped PEI preform. (b) SEM micrograph illustrating cross-sections of (i) 200 μm and 500 μm sized fibers with 20 parallel equilateral v-grooves (scale bar: 100 μm), and (ii) 500 μm size fiber showing the textured microgrooves that form microchannels which extend along its entire length (scale bar: 100 μm). (c) SEM micrographs of a coated fiber showing homogeneously coated nanoparticles (scale bars: 15 μm and 1.5 μm (inset)). (d) AFM micrographs of uncoated and nanoparticle coated fibers. Nanoparticle coating introduces a random nanoscale roughness on the ordered microscale roughness of the fiber surfaces (scale bars: 0.5 μm).

ORMOSIL nano-particles (with sizes around 10 nm) interconnect to constitute a porous network (ESI Fig. S2d†).

Surface roughness (RMS) of PEI smooth fiber increased from 3 nm to about 50 nm when coated with ORMOSIL as measured from AFM micrographs (Fig. 2d). After spray coating, a hierarchical surface structure with micro-scale grooves and nanoparticles were introduced on the fiber surface. It is apparent that the surface roughness is magnified due to the nanoparticle coating. Consequently, this enhances the wetting properties of liquid droplets on the surfaces. As reported, the coated ORMOSIL film is durable over flexible substrates when subjected to bending, and its hydrophobicity is not affected by the environmental pH. Moreover, mechanical durability of the coated film was investigated by water dripping and adhesive tests.[33,34] After dripping water drops (~100 μL) for about 1 h, the film remained superhydrophobic (CA ~ 156°). In the case of adhesive tape, the surface was destructed where remnant of adhesive material sticks to the films upon detachment. Contact angle can be easily increased close to 180° by using methanol as solvent for gel synthesis as we reported in our previous work.[37] However, increasing the contact angle decreases the anisotropy of the fiber arrays. The ORMOSIL coatings used in this work were optimized to obtain superhydrophobicity with good anisotropy.

### Surface characterization of fiber arrays

Arrays of fibers with different surface properties were prepared to study anisotropic wetting/non-wetting behavior of the fibers. Uncoated smooth, uncoated grooved, nanoparticle coated smooth, and nanoparticle coated grooved fibers of PEI and PC (each 8 cm in length and 300 μm in diameter) were fixed firmly on glass substrates using a double sided adhesive tape to form surfaces (Fig. S4a†). Static CA of water droplets (4 μL) were measured from directions parallel and perpendicular to fibers' orientation at ambient environment (Fig. 3a). Water droplet resting on the uncoated smooth PEI fiber surfaces was in Wenzel state and fills the spaces between the fibers (Fig. 3b-i). After surface modification by coating ORMOSIL, smooth fiber surface gained additional nano-scale roughness, and the CA values increased in both parallel and perpendicular directions (Fig. 3b-ii). The droplet resting on the surface was not in homogeneous wetting state, rather it was in the intermediate state where inhomogeneity exist due to nano-roughness. But, it has not attained complete inhomogeneous wetting as in Cassie state. The uncoated grooved fiber surface has two very ordered roughness scales ascribed by the parallel grooves and the fibers, and therefore hydrophobicity is magnified on the surface even without the nanoparticle coating. Also, CA was increased in both parallel and perpendicular directions because of the groove morphology. On the uncoated grooved surface, water cannot fill the spaces between the fibers, but can penetrate the micro-grooves structures on the fibers (Fig. 3b-iii). However, the nanoparticle coated grooved fibers demonstrated hydrophobicity with enhanced CA in both parallel and perpendicular directions due to the introduced nano-scale roughness apart from their surface chemistry. Composite of solid/air is formed when a droplet rest on the surface with pseudo spherical shape.

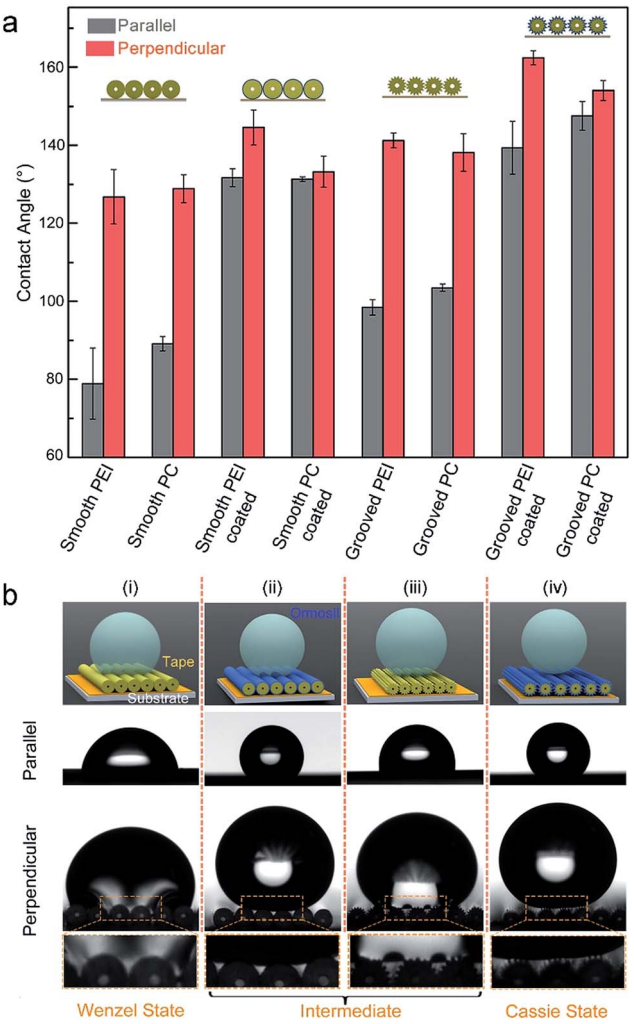


Fig. 3 (a) Contact angle measurements of fiber array surfaces (with each fiber 8 cm in length and 300 μm in diameter) with 4 μL water droplets. The measurements were taken from parallel and perpendicular directions, which correspond to the directions with respect to the fiber orientation of the surfaces. (b) Photographs showing the wetting behavior on PEI fiber surfaces. (i) The droplet on uncoated smooth fibers is in the Wenzel state, where spaces within the fibers are filled with water as seen in the inset. For nanoparticle coated smooth or uncoated grooved fiber surfaces, the droplets are in an intermediate state between Cassie and Wenzel states. (ii) The smooth fiber surface is wet, but the water cannot penetrate the in-fiber spaces for the array of coated smooth fibers. (iii) For the case of uncoated grooved fibers, water filled the micro-channels within the microscale grooves yet cannot wet the spaces between the fibers as seen from the inset. (iv) The droplet is in the Cassie state on nanoparticle coated grooved fibers. The water droplet rests on the tips of groove protrusions on the fibers and water cannot penetrate the grooves or the spaces between fibers.

Trapped air beneath the droplet minimizes the contact area between the solid surface and the liquid. It is observed that water neither fill the space between the fibers nor penetrate the grooves of the fiber due to the combined effect of surface chemistry and multi-scale roughness (Fig. 3b-iv). In addition, evident of the contribution chemical and nanoroughness was provided to reveal the effectiveness of nanoparticle coating on

the fiber grooves by measuring CA on glass and polymer (PC and PEI) substrates as reference (Fig. S4b†). With a considerable degree of accuracy, we then, recognize a distinction between the CA revealed by surfaces when coated with ORMOSIL nanoparticles. The same reasoning applies for the grooved PC and PEI fibers. It is inherent in the fundamental theory of wetting that roughness enhances the CA of liquid on solid. This is an evidence we observed on the fiber surfaces. The superhydrophobicity on the coated fibers ensued from nano-scale roughness introduced by the coatings and fiber surface chemistry.

### Comparison of anisotropic behavior on PC and PEI fiber arrays

The fibers (grooved or smooth) are principally a roughness scale with pristine anisotropic behavior when they form an array. The aligned fibers and parallel grooves introduce a very ordered roughness hierarchy. The uncoated smooth PEI and PC fiber surfaces exhibit CA difference of 48° and 39° respectively. By definition, CA difference is the change in the parallel and perpendicular CA measured on the fiber surfaces. The CA difference reveals the anisotropic wetting property of the fibers due to the very ordered surface topography induced by the parallel aligned grooves on the fiber. Relative to the smooth fibers, anisotropy was observed on the grooved PEI and PC fibers with greater CA. When compared to the grooved fiber, water droplet spreads isotropically on the bare PEI and PC films. Moreover, in expense of the nanoroughness introduced by coating, the anisotropy of the coated grooved PC and PEI diminished and the difference of CA in parallel and perpendicular direction was reduced. On the basis of wetting resistance considering a drop resting on the coated grooved PEI and PC fiber arrays, relatively the highest CA of 162° was observed on the coated grooved PEI fiber compared to 154° on coated grooved PC fiber array (Fig. 3a). In addition to the magnified wetting property of the surfaces, a substantial anisotropy is

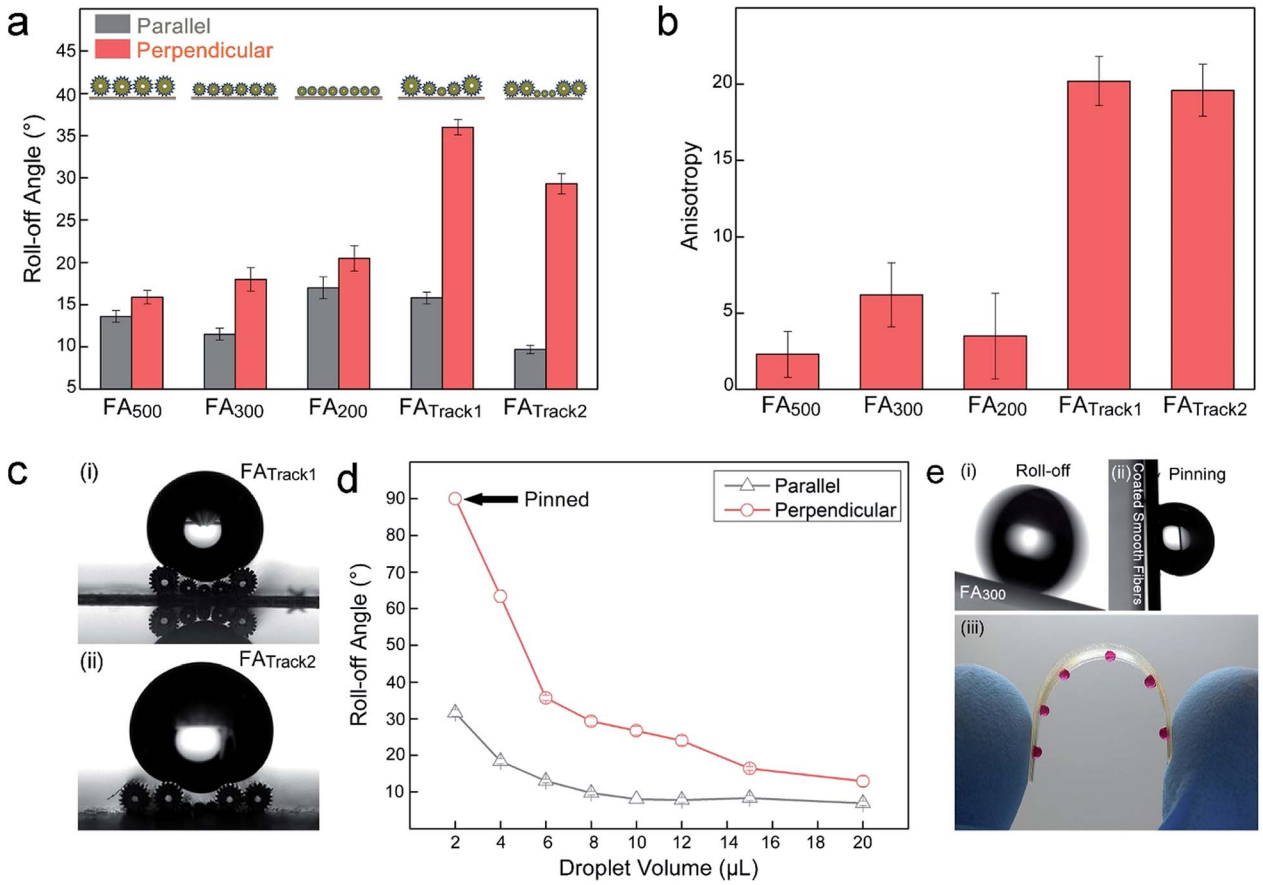


Fig. 4 (a) Roll-off angle values measured on ORMOSIL coated grooved fiber arrays (FA) formed by fibers with diameters of 500 μm, 300 μm and 200 μm ($FA_{500}$, $FA_{300}$ and $FA_{200}$), and their combinations ($FA_{Track1}$ and $FA_{Track2}$). (b) Anisotropy ($\Delta\theta = SA_{\perp} - SA_{\parallel}$) of the fiber arrays, showing enhanced anisotropic non-wetting behavior on $FA_{Track1}$ and $FA_{Track2}$ surfaces. (c) Photographs of droplets on $FA_{Track1}$ and $FA_{Track2}$. (i) $FA_{Track1}$ is a parabolic array of 500 μm/300 μm/200 μm/300 μm/500 μm fibers. (ii) $FA_{Track2}$ is a channel composed of 500 μm × 2/200 μm × 3/500 μm × 2 array. (d) The relation between roll-off angle and droplet volume on $FA_{Track2}$. Roll-off angle decreases with increasing droplet volume in both parallel and perpendicular directions. However, roll-off angle is higher in the perpendicular direction for all droplet volumes, which demonstrates the anisotropic non-wetting behavior of the surface. (e) Roll-off and adhesive properties of nanoparticle coated smooth and grooved fiber surfaces. (i) Anisotropic roll-off in parallel direction on the $FA_{300}$ surface tilted at 14°. (ii) The droplet remains pinned to a nanoparticle coated fiber surface with 300 μm smooth fibers even when the surface is tilted at 90°. (iii) Pinned droplets on a flexible substrates for conceptual demonstration.

revealed alongside directional superhydrophobicity. In the sense of anisotropy, the coated grooved PEI fiber revealed greater tendency of directional nonwetting within the entire range of the fiber arrays which we believe is due to differences in the intrinsic surface chemistry between PEI and PC. Therefore, PEI is preferably utilized in the proceeding part of the work that followed.

Variation in groove dimension also affects the surface wetting property of the fibers. Combination of microgroove with nanoparticle improves the nonwetting behavior significantly. When the fibers are not coated with nanoparticle, the contribution to hydrophobicity is mainly from the intrinsic surface chemistry of the polymer fiber and the grooves. Dimension of the fibers varies on polymer fibers with different diameters as a result of the reduction factor of the original preform during drawing. For example, fiber with 500 μm diameters have grooves with 50 μm height and 70 μm gap between grooves. Fibers with 300 μm size have grooves with 30 μm height and 50 μm gap. CA of the uncoated grooved PEI surfaces reveals that, variation in the groove dimension does not affect the CA significantly irrespective of fiber size (Fig. S5a†). However, for coated grooved PEI fibers, the anisotropy is greater on both 200 and 300 μm size fibers than on 500 μm size fibers (Fig. S5b†). It was clearly observed that number of groove in intimate contact with the droplet varied on these surfaces. Since fewer number of grooves were in contact with the droplet on the surfaces composed of 500 μm fiber due to the larger size of the fiber, the elongation of the droplet was less compared to the surfaces composed of 200 μm and 300 μm. A key practical explanation was noticed in the differences of the CA measured in parallel and perpendicular directions on the surfaces.

We investigated rice leaf-like directional roll-off of water droplets from the fiber surfaces with roll-off angle measurements from parallel and perpendicular directions using 8 μL of water droplets. Surfaces and tracks with a variety of topographies were designed by employing nanoparticle coated grooved fibers with varying diameters (200 μm, 300 μm and 500 μm) as building blocks. Initially, three different fiber arrays of 200 μm, 300 μm and 500 μm sized grooved fibers coated with ORMOSIL nanoparticles were constructed and labeled as $FA_{500}$, $FA_{300}$, and $FA_{200}$ (Fig. 4a). All of these three surfaces were slightly anisotropic with a roll-off angle differences around 5° between parallel and perpendicular directions. This difference in roll-off angle ($\Delta\theta = SA_{\perp} - SA_{\parallel}$) is referred to as the anisotropy of the surfaces, and is shown for each surface in Fig. 4b. To improve the anisotropic roll-off behavior, combinations of different sized fibers were used to obtain surfaces that demonstrate greater anisotropic non-wetting behavior. The fibers with 500 μm, 300 μm and 200 μm sizes were used to prepare a parabolic fiber array (track), which is labeled as '$FA_{Track1}$' (Fig. 4c-i). This surface pattern demonstrated a greatly enhanced anisotropic behavior with anisotropy of about 20°. Another track pattern (labeled as '$FA_{Track2}$') was prepared using 500 μm and 200 μm sized fibers (Fig. 4c-ii). The anisotropy was about 20° for this surface. In addition, we studied the effect of water droplet size on anisotropic roll-off behavior using $FA_{Track2}$ (Fig. 4d). Both the roll-off angle and the $\Delta\theta$ decrease with increasing droplet volume. The ordered hierarchical roughness of the fibers and the grooves become less effective with increasing droplet volumes. However, the roll-off value is smaller in parallel direction for all droplet volumes, which demonstrates that anisotropic non-wetting behavior is retained. On the other hand, when droplet volume is too small, it pinned to the surface. For instance, droplet of 2 μL size pinned to the surface in perpendicular direction but not in the parallel direction. Furthermore, we compared the roll-off phenomenon on nanoparticle coated smooth and grooved fibers to clarify the surface behavior difference contributed by the on-fiber groove structures. Fig. 4e-i and ii show a droplet rolling off a 300 μm coated grooved fiber surface at a roll-off angle of 14°, and a droplet pinned to a coated smooth fiber surface at a tilting angle of 90°. Red colored water droplets are distributed on a flexible substrate as an array (Fig. 4e-iii).

## Droplet manipulation on fiber arrays and tracks

Using the surface textured fibers as building blocks, we prepared surfaces for micro-droplet transport, guiding, and mixing. Fig. 5 shows the transport of water droplets and their controlled mixing using arrays of textured fibers. In Fig. 5a,

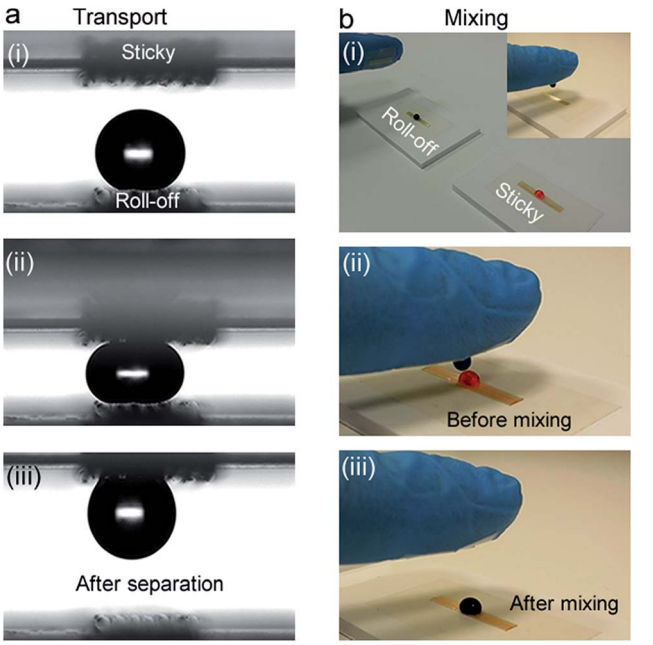


Fig. 5 Droplet transport and mixing. (a) Snapshots of a 4 μL suspended droplet on the roll-off superhydrophobic fiber surface (array of 300 μm coated grooved fibers). The droplet is transferred from the superhydrophobic surface to the sticky hydrophobic surface (array of nanoparticle coated 300 μm fibers) upon bringing the two surfaces in close proximity. (b) Droplet transportation with fiber surfaces prepared on arbitrary surfaces. (i) An array of 300 μm coated smooth fibers was prepared on the fingertip of a nitrile glove. By gently touching the resting blue dyed water droplet (on the 300 μm nanoparticle coated grooved fiber surface), it was transferred to the fingertip. (ii) The blue droplet was carried on the fingertip and was contacted with the red dyed droplet resting on a sticky surface manually. (iii) The resulting droplet after mixing of the initial red and the blue droplets.

steps of droplet transport from a roll-off superhydrophobic surface (array of 300 μm coated grooved fibers) to a sticky hydrophobic surface (array of 300 μm coated smooth fibers) was demonstrated. When the droplet sitting on the roll-off surface was gently squeezed with the upper sticky hydrophobic surface, it pinned to the sticky surface after relaxation. Since the fibers are flexible, it is possible to prepare fiber arrays on arbitrary surfaces. For instance, Fig. 5b demonstrates controlled water droplet mixing using a sticky hydrophobic fiber array constructed on the fingertip of a nitrile glove. A person wearing this glove can manually transport a water droplet (blue) sitting on a roll-off superhydrophobic surface to the array of sticky hydrophobic fibers on her/his finger (Fig. 5b-i). The droplet can be carried on the fingertip and merged with another droplet (red) by gently touching the second droplet (Fig. 5b-ii and iii).

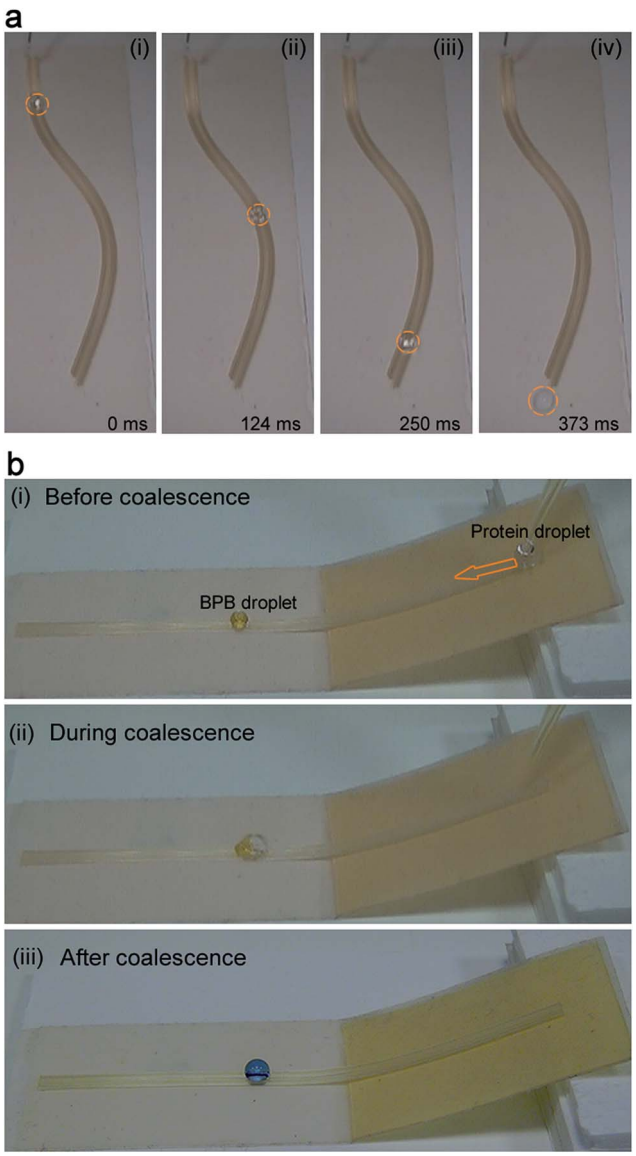


Fig. 6 (a) Snapshots of a droplet rolling on the curved fiber track ($FA_{track2}$) taken with a high-speed camera. Water droplet followed the curved path outlined by the fibers at a roll-off angle of around 11°. (b) A droplet based protein assay for colorimetric detection on linear fiber tracks. (i) Dispensing yellow BPB and colorless protein solution (8 μL and 9 μL, respectively). (ii) The instant of the droplet collision. (iii) Color change after coalescence of the two droplets. The yellow color of BPB solution changed to blue after mixing with the protein solution.

We constructed a curved 8 cm long $FA_{track2}$ path to demonstrate droplet manipulation for open microfluidic channels. Water droplets (8 μL) were guided successfully along the curved path by tilting the surface to about 10° (Video S1†). Snapshots in Fig. 6a show the positions of the water droplet at different time intervals on the track. The water droplet was guided within the channel without leaving the designed path until the end of the track.

Lastly, we demonstrate a proof of principle protein assay based on droplet coalescence on a linear track with one side slightly raised to make an angle of 11° with the substrate. A 9 μL colorless droplet of human serum albumin (HSA) protein solution (5 mg $mL^{-1}$ in PBS, pH 7.4) was rolled from the slope formed by the track and collided with the 8 μL yellow droplet of bromophenol blue (BPB) dye (0.1 mg $mL^{-1}$ BPB in glycine buffer (10 mM) at pH 2.3), as shown in Fig. 6b-i and ii. The droplets coalesced into a larger droplet (mixture of HAS and BPB solutions) on the track. A color change of the resulting droplet was detected immediately, and yellow color of BPB changed to blue completely in 8 seconds after the coalescence (Fig. 6b-iii).

## Conclusions

We demonstrated a simple fabrication of rice leaf inspired anisotropic non-wetting surfaces using surface textured polymer fibers. A high throughput and well established top down thermal drawing method was applied to produce several meters long fibers with perfectly aligned parallel microscale v-grooves. We highlight the capability of the thermal drawing method to several engineering polymers including polycarbonate and polyetherimide. Fiber pieces of varying lengths were fixed on substrates using double sided tape to form large area anisotropic surfaces. Nanoscale random roughness was added to the ordered microscale topography on the surfaces by spray coating a hydrophobic ORMOSIL suspension. The anisotropic wetting/non-wetting characteristics of the surfaces were investigated with contact angle and roll-off angle measurements in both parallel and perpendicular directions to the fibers' orientation. By use of the structured fibers as building blocks, we prepared track designs to show the promising potential of the surface textured fibers in the area of droplet manipulation. In the future, we aim at understanding how different geometries will affect the wetting properties of the fiber. We believe this research can pave the way for wide potential applications such as directional self-cleaning surfaces, droplet microfluidics, fog collection, and non-wetting textiles.

## Acknowledgements

We thank Abubakar Isa Adamu for fruitful discussions and Pinar Beyazkilic for preparation of ORMOSIL colloid. This work is partly supported by TUBITAK under the Project No. 111T696. The research leading to these results has received funding from

the European Research Council under the European Union's Seventh Framework Programme (FP/2007-2013)/ERC Grant Agreement no. 307357.

## References

1 D. Xia and S. R. J. Brueck, *Nano Lett.*, 2008, **8**, 2819.
2 N. A. Malvadkar, M. J. Hancock, K. Sekeroglu, W. J. Dressick and M. C. Demirel, *Nat. Mater.*, 2010, **9**, 1023.
3 M. J. Hancock and M. C. Demirel, *MRS Bull.*, 2013, **38**, 391.
4 P. Zhang, H. Liu, J. Meng, G. Yang, X. Liu, S. Wang and L. Jiang, *Adv. Mater.*, 2014, **26**, 3131.
5 T. A. Duncombe, E. Y. Erdem, A. Shastry, R. Baskaran and K. F. Böhringer, *Adv. Mater.*, 2012, **24**, 1545.
6 V. Liimatainen, V. Sariola and Q. Zhou, *Adv. Mater.*, 2013, **25**, 2275.
7 Y. Zheng, X. Gao and L. Jiang, *Soft Matter*, 2007, **3**, 178.
8 X. Gao and L. Jiang, *Nature*, 2004, **432**, 36.
9 X. Q. Feng, X. Gao, Z. Wu, L. Jiang and Q. S. Zheng, *Langmuir*, 2007, **23**, 4892.
10 D. Wu, J. Wang, S. Wu, Q. Chen, S. Zhao, H. Zhang, H. Sun and L. Jiang, *Adv. Funct. Mater.*, 2011, **21**, 2927.
11 S. G. Lee, H. S. Lim, D. Y. Lee, D. Kwak and K. Cho, *Adv. Funct. Mater.*, 2013, **23**, 547.
12 D. Xia, L. M. Johnson and G. P. Lopez, *Adv. Mater.*, 2012, **24**, 1287.
13 E. Bittoun and A. Marmur, *Langmuir*, 2012, **28**, 13933.
14 J. Groten and J. Ruhe, *Langmuir*, 2013, **29**, 3765.
15 V. Jokinen, M. Leinikka and S. Franssila, *Adv. Mater.*, 2009, **21**, 4835.
16 Q. F. Xu, J. N. Wang, I. H. Smith and K. D. Sanderson, *Appl. Phys. Lett.*, 2008, **93**, 233112.
17 H. Mertaniemi, V. Jokinen, L. Sainiemi, S. Franssila, A. Marmur, O. Ikkala and R. H. A. Ras, *Adv. Mater.*, 2011, **23**, 2911.
18 H. Mertaniemi, R. Forchheimer, O. Ikkala and R. H. A. Ras, *Adv. Mater.*, 2012, **24**, 5738.
19 X. Yao, Y. Song and L. Jiang, *Adv. Mater.*, 2011, **23**, 719.
20 S. M. Kang, C. Lee, H. N. Kim, B. J. Lee, J. E. Lee, M. K. Kwak and K. Y. Suh, *Adv. Mater.*, 2013, **25**, 5756.
21 J. Y. Chung, J. P. Youngblood and C. M. Stafford, *Soft Matter*, 2007, **3**, 1163.
22 J. H. Lee, H. W. Ro, R. Huang, P. Lemaillet, T. A. Germer, C. L. Soles and C. M. Stafford, *Nano Lett.*, 2012, **12**, 5995.
23 Y. Li, S. Dai, J. John and K. R. Carter, *ACS Appl. Mater. Interfaces*, 2013, **5**, 11066.
24 P. C. Lin and S. Yang, *Soft Matter*, 2009, **5**, 1011.
25 F. Zhang and H. Y. Low, *Langmuir*, 2007, **23**, 7793.
26 D. Xia, X. He, Y. B. Jiang, G. P. Lopez and S. R. J. Brueck, *Langmuir*, 2010, **26**, 2700.
27 H. Wu, R. Zhang, Y. Sun, D. Lin, Z. Sun, W. Pan and P. Downs, *Soft Matter*, 2008, **4**, 2429.
28 J. Yong, Q. Yang, F. Chen, D. Zhang, U. Farooq, G. Du and X. Hou, *J. Mater. Chem. A*, 2014, **2**, 5499.
29 F. Chen, D. Zhang, Q. Yang, X. Wang, B. Dai, X. Li, X. Hao, Y. Ding, J. Si and X. Hou, *Langmuir*, 2011, **27**, 359.
30 D. A. Boyd, A. R. Shields, J. Naciri and F. S. Ligler, *ACS Appl. Mater. Interfaces*, 2013, **5**, 114.
31 D. A. Boyd, A. R. Shields Jr, P. B. Howell and F. S. Ligler, *Lab Chip*, 2013, **13**, 3105.
32 A. Yildirim, M. Yunusa, F. E. Ozturk, M. Kanik and M. Bayindir, *Adv. Funct. Mater.*, 2014, **24**, 4569.
33 A. Yildirim, H. Budunoglu, M. Yaman, M. O. Guler and M. Bayindir, *J. Mater. Chem.*, 2011, **21**, 14830.
34 A. Yildirim, T. Khudiyev, B. Daglar, H. Budunoglu, A. K. Okyay and M. Bayindir, *ACS Appl. Mater. Interfaces*, 2013, **5**, 853.
35 R. N. Wenzel, *Ind. Eng. Chem.*, 1936, **28**, 988.
36 A. B. D. Cassie and S. Baxter, *Trans. Faraday Soc.*, 1944, **40**, 546.
37 H. Budunoglu, A. Yildirim, M. O. Guler and M. Bayindir, *ACS Appl. Mater. Interfaces*, 2011, **3**, 539.



 